IEEE Access
Multidisciplinary | Rapid Review | Open Access Journal

Received May 11, 2021, accepted May 23, 2021, date of publication May 26, 2021, date of current version June 7, 2021.

Digital Object Identifier 10.1109/ACCESS.2021.3083960

Enhancement of Frequency Control for Stand-Alone Multi-Microgrids

KAVITA SINGH[1], (Student Member, IEEE), MOHAMMAD AMIR[1], (Student Member, IEEE), FURKAN AHMAD[2], (Member, IEEE), AND SHADY S. REFAAT[3], (Senior Member, IEEE)

[1]Department of Electrical Engineering, Faculty of Engineering and Technology, Jamia Millia Islamia (Central University), New Delhi 110025, India
[2]Centre for Automotive Research and Tribology (CART), Indian Institute of Technology Delhi, New Delhi 110016, India
[3]Department of Electrical Engineering, Texas A&M University at Qatar, Doha, Qatar

Corresponding author: Shady S. Refaat (shady.khalil@qatar.tamu.edu)

This work was supported by the Qatar National Library.

ABSTRACT This paper presents dual-stage fractional order PID controller to enhance the primary frequency regulation of interconnected multi-μgrids in standalone mode. A rational, non-integer ordered calculus-based controller is assessed via a single-area microgrid system pursued by a two-area microgrid to integrate a tidal power plant (TPP). Additionally, it is employed with conventional units in frequency control to certify system steadiness. Thus, a strategy to showcase the contribution of TPP in frequency regulation with the integration of the diesel engine power plant is proposed. Also, the proposed methodology shows the support of TPP in primary frequency regulation strategies such as inertia, damping control, and supplementary control with deloading activity. For getting superior outcomes and enhanced steadiness of the microgrid, the controller gains are streamlined utilizing an imperialist competitive algorithm (ICA). To demonstrate the efficiency of ICA, The obtained results are compared with the genetic algorithm and particle swarm optimization algorithm. The proposed investigation is conducted in single-area and two-area microgrid systems through MATLAB simulation verification. The obtained results prove the effectiveness of the proposed methodology.

INDEX TERMS Deloaded tidal turbines, frequency control, microgrid, fractional order controller, tidal power plant.

NOMENCLATURES

D_a	Additional damping
M_a	Additional inertia
β	Blade pitch angle
K_{pd}	Diesel engine generator proportional constant
K_{id}	Diesel engine generator integral constant
K_{dd}	Diesel engine generator derivative constant
P_L	Demanded load
DEG	Diesel Engine Generator
D_1/D_2	Damping constant of $\text{Area}_1/\text{Area}_2$
DERs	Distributed Energy Resources
P_e	Electrical power
λ	Fractional order of M_a
μ	Fractional order of K
FOPID	Fractional Order Proportional-Integral-Derivative
ΔF	Frequency deviation
GA	Genetic Algorithm
H	Inertia constant of tidal power plant
ICA	Imperialist competitive algorithm
M_1/M_2	Inertia constant of system $\text{Area}_1/\text{Area}_2$
MPP	Maximum Power Point
w^*_{ref}	Mechanical reference rotational speed
w_m	Mechanical rotational speed
J	Moment of inertia of the rotating mass
P_m	Mechanical power
T_m	Mechanical torque
C_{TT}	Power coefficient
P_{del}	The power output of Tidal turbine generator at deloading operating point
PID	Proportional– integral– derivative
P_{TT}	Power generated on the tidal turbine shaft
K_{pp}	Pitch angle control proportional constant
K_{ip}	Pitch angle control integral constant
K_{dp}	Pitch angle control derivative constant

The associate editor coordinating the review of this manuscript and approving it for publication was Muhammad Tariq.

This work is licensed under a Creative Commons Attribution 4.0 License. For more information, see https://creativecommons.org/licenses/by/4.0/

PSO	Particle swarm optimization
P_{max}	Rated maximum power of tidal turbine generator
Tr	Rated turbine torque (tidal)
ω_{blade}	The rotational speed of blades
R_{blade}	The radius of the turbine blades
P_{ref}	Reference power of tidal turbine generator
ω_{del}	Rotor speed at deloading operation point
w_r	Rated rotor speed
K_{ps}	Speed regulator proportional constant
K_{is}	Speed regulator integral constant
$R1$, $R2$	Speed regulation constant (in Hz/pu MW)
K_{sys}	System frequency characteristic constant of the system
A_{TT}	The swept area of the rotor
K	Supplementary control
TTG	Tidal Turbine Generator
T_{DT}	Turbine time constant
$\frac{dp}{d\beta}$	Tidal output deviation for a definite change of blade angle
$\frac{dp}{dV}$	Tidal output deviation for a specific tidal speed change
$\frac{dp}{d\omega}$	Tidal power deviation to the small change of turbine angular speed
T_{DG}	The time constant of the governor
T_w	The time constant of the washout filter
P_s	Total power generation by TTG and DEG
V_{TT}	Tidal rated speed in m/sec
λ_{TT}	Tip-speed ratio
Tpp	Tidal power plant
T_{TT}	Tidal turbine time constant
ρ_{TT}	Water density

I. INTRODUCTION

Recently, the utilization of tidal power has acquired a lot of consideration. It can provide a substantial electrical power asset as the sea covers around 70% of the earth. TPP shows a vast potential of electrical power extract from the sea without disturbing nature and might compete with other sustainable energy sources, such as wind and solar. TPP is exceptionally valuable for seaside locations away from the vast accessibility of tidal resources. It might be viewed as an economical way to provide power while working in parallel with conventional resources. The workability of TPP requires a gap amid height/peak of elevated, and ebb tides must exceed five meters based on studying numerous sea locations. The introduction of sustainable sources such as tidal or wind power sources demands efficient frequency regulation, which needs to be considered in reconstructing the modern power systems [1].

Tidal stream power is fluctuating in nature. Thus, power electronics devices are required to provide the decoupling of TPP from an infinite bus system. Generally, these generation units do not contribute to frequency regulation. It implies that these units are not contributing to system inertia and, consequently, bring about large frequency deviation (Δf) for unbalance in demand and supply [2]. TPP operates at the maximum power point (MPP) to disengage the highest accessible energy through the tidal stream. Varying speed TPP is adopted in this present study. To ensure effective participation of TPP in the frequency regulation process, an approach of deloaded activity from maximum power point might be employed to create a sufficient power reverse margin. Various cases have been discussed on wind power plants (WPP) [3]–[5]. In [3], the deloaded activity in TPP for dynamic energy participation can be accomplished by moving the operational zone from its maximum power zone to a decreased capacity zone. These reverse power margins might be utilized to achieve stability between load and supply.

The turbine speed can be incremented above/over an allowable range under the permissible bound by pitch angle regulation by utilizing the deloading concept [4]. Similarly, in [5], the deloaded TPP has been utilized the pitch regulation strategy for limiting the ΔF. Therefore, another methodology has been proposed in [6] for the single-area power model's frequency regulation. The authors proposed a scheme that utilizes an additional inertial integration of WPP to synchronize with conventional generating units. Under this methodology, WPP is involved to keep up the inertia estimate at the desired level and improves the model's transient steadiness. In [7], the effect of demoted inertial and its controlling technique has been proposed to eliminate the unpredicted frequency deviation in the modernized power system.

In [8] and [9], the authors have introduced an additional damping controlling method in the interconnected power system. Several research works have been conducted on the primary frequency regulation through WPP by deloaded process. It has been testified in short/long-term frequency regulations. As seen from the literature survey, few works are done in frequency regulation using deloaded activity of TPP. Thus, for enhancing the frequency regulation in TPP based microgrid system, pitch control of the deloaded TPP in frequency control is executed. TPP with a deloaded operation might do excellent work in frequency control with the integration of diesel power plant (DPP) considering both primary and secondary frequency control strategies.

Therefore, a dynamic model of the load frequency control for a single area microgrid and two area microgrid utilizing TPP and DPP is proposed. The investigation of frequency response for short-duration support of TPP in frequency regulation by adopting additional inertia and damping controlling strategies is conducted.

The additional inertia, damping control, and supplementary control are realized through a fractional order controller (dual stage FOPID (1 + PI)). The proportional derivative (PD) part provides the additional damping and inertia. The integral part (I) gives supplementary control to the power system. Thus, the derivative part of the controller improves the transient performance and necessarily enhances the system's steady-state response by reducing steady-state error [11]. There are many research challenges related to

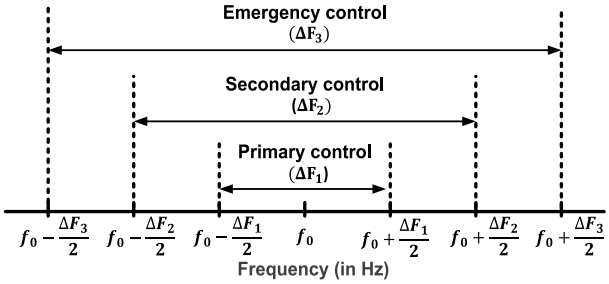

FIGURE 1. Frequency map and control actions.

the activity and controlling of the independent microgrid in the presence of TPP (random power source). Despite the diversity of solutions tackling these challenges, they become complex. The fluctuating tendency of TPP may cause Δf due to the gap amid demand and supply. These fluctuations can harm devices and may lead to a power system breakdown. Because of the acknowledged standard of ΔF (see Fig. 1) [12], an investigation on essential controlling activities, for example, primary/secondary/ emergency control of the integrated wind system, is executed by [13].

Similarly, numerous operation-related challenges can be resolved by interconnecting two or more microgrid systems. However, there are significant advantages associated with interconnecting the microgrids, such as an exchange of power under the nominal working condition and crises, a decrease of fundamental power reverse margin limit, adaptability to construct a bigger power plant, and progressively solid and stable activity are executed efficiently.

Although a vast literature has been developed to control the frequency regulation in conventional units [14]–[16], and non-conventional units [17]–[20] based on multi-area power systems. Therefore, in this investigation, the frequency regulation is analyzed in two area microgrid systems comprising TPP and DPP with a frequency regulation provided by deloaded TPP. Recently, researchers have been focusing on optimization methods for the tuning of various parameters of the controller utilized in frequency regulation. In [21], the authors have utilized the PSO method to optimize the PID controller's gains for frequency regulation in a multi-area power system. In [22], the authors have employed GA to tune the parameters of the controller in a hybrid system. A detailed investigation of frequency regulation of isolated hybrid power system/two-area hybrid system utilizing a Quasi-oppositional harmony search algorithm (QOHSA) has been proposed in [23].

The literature review indicates that a lot of research work has been conducted to find novel optimization methods or further enhancing solutions for different engineering issues like load frequency control, process control, etc. ICA is one of the best algorithms for tuning the controller's various design parameters in the load frequency control field [24]. ICA is a powerful, effective, and recent evolutionary algorithm employed in [25], [26]. This algorithm mimics the imperialistic competition process. The authors of the proposed study have used the ability of ICA to search the optimal parameter values of the controllers engaged with TPP-based single/two area microgrids for frequency regulation. The outcomes yielded from the proposed approach are compared with other existing algorithms. In summary, the main contributions of the paper include the following.

- Although extensive studies of enhancing the frequency regulation for standalone multi-microgrid have been conducted, there are several gaps in implementing an effective control method. Thus, the main contributions of this paper are summarized below. Analysis of frequency control for TPP and DPP units based on the isolated microgrid for interconnecting two area microgrid is performed.
- The transient involvement of deloaded TPP in primary frequency control utilizing pitch angle controller is presented.
- The impact of additional inertia, damping, and supplementary control on the performance examination of the considered microgrid model's frequency regulation is investigated.
- The performance of the proposed control strategy is compared with existing techniques, i.e., FOPID/PID, to show the effectiveness in transient response.
- ICA is utilized for optimizing the parameters of all controllers used in the proposed microgrid to acquire excellent performance.
- The efficiency of the ICA is investigated with other contemplated algorithms.

The remaining of the paper is organized as follows. Section 2 discusses the mathematical model of TPP and DPP units. Section 3 provides a detail of the proposed controller. The deloaded activity of TPP is talked about in Section 4. The proposed controlling methodology is informed in section 5. Section 6 provides a detailed dynamic model of TPP-based microgrids. In Section 7, a performance index plan is presented. The proposed ICA is given in Section 8. The results analysis is presented in Section 9, trailed by the conclusion, and discussions are presented in Section 10.

II. MATHEMATICAL DESCRIPTION OF TPP

This section deals with a developed mathematical model. It is built in MATLAB/Simulink environment for the tidal turbine and power generation system. The developed mathematical model is used for generating the power output of TPP.

A. TIDAL TURBINE GENERATOR (TTG)

The total kinetic power available on a tidal turbine shaft is defined by Eq. (1) as given in [10].

$$P_{TT} = \frac{1}{2}\rho_{TT} A_{TT} C_{TT} V_{TT}^3 \tag{1}$$

where ρ_{TT} is the water density, A_{TT} is the swept area of the rotor, V_{TT} is the tidal rated speed in meter per sec, and C_P is the power coefficient. It depends upon the pitch angle of the

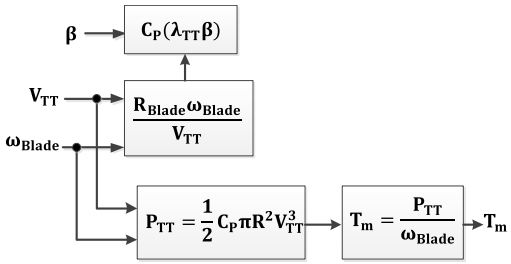

FIGURE 2. Block diagram of tidal turbine.

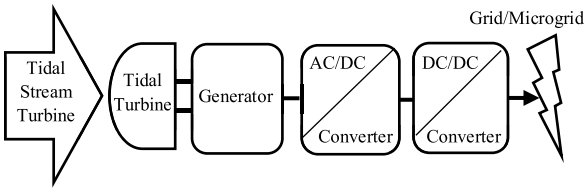

FIGURE 3. The tidal power generation system.

blades (β), and the tip-speed ratio (λ_{TT}) is written as [10]:

$$C_P = (0.44 - 0.0167\beta)\, sin\left[\frac{(\lambda_{TT} - 3)}{15 - 0.3\beta}\right] - 0.0184\,(\lambda_{TT} - 3)\,\beta \quad (2)$$

Hence, $\lambda_{TT} = {R_{blade}\omega_{blade}}/{V_{TT}}$, and $R_{blade}\,/\omega_{blade}$ = radius of the turbine blades/rotational speed of blades. The torque produced by the tidal turbine is defined by Eq. (3).

$$\mathrm{Tm} = P_{TT}/\omega_{blade} \quad (3)$$

By considering the mathematical equations established previously, the block diagram of the developed turbine model is shown in Figure 2. The tidal turbine is adapted to the generator via a gearbox, as shown in Figure 3. Tidal power is converted into electrical power (tidal turbine and generator)—the three-phase variable AC output.

The tidal turbine is adapted to the generator via a gearbox, as shown in Fig 3. Tidal power is converted into electrical power (tidal turbine and generator). The variable AC (three-phase) output of the tidal generator is converted into variable DC voltage. The variable DC output voltage of the diode bridge is connected to a DC-DC boost converter. The output of the DC-DC boost converter is a constant DC bus. The constant DC bus voltage is converted into three-phase AC at 60 Hz.

B. OPERATIONAL MODES OF TTG

TTG model is designed to work in four modes of operation with specific limits of tidal speed. Tidal speed ranges are divided as cut-in speed/ rated speed/cut-out speed, as revealed in Figure 4, and the description is given as [27].

Operational zone 1- In this zone, the power output by TTG is zero. It is known as an uneconomical operational zone. The pitch angle is fixed to 90^0.

Operational zone 2-In this zone, tidal speed is present between cut-in speed and rated speed. It is also known as the maximum power yield zone due to the maximum efficiency

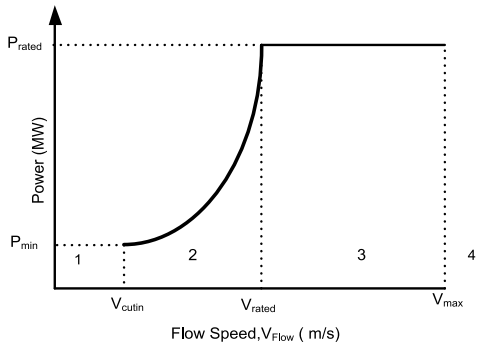

FIGURE 4. Power output curve of tidal turbine.

of TTG to take out power from the tidal wave. In this study, TTG (in deloaded mode) works in this zone with a pitch angle fixed to 3^0.

Operational zone 3- -In this zone, the tidal speed is present between rated speed and cut-out speed. It is also known as the constant power zone. In this region, the pitch angle varies in the bound of 3^0 to 90^0.

Operational zone 4-In this zone, the speed of the tidal is above the cut-out range. The power output is nil. In this study, TTG is controlled by pitch angle strategy, similarly employed in wind turbines. They primarily work focused on the regulation of primary frequency through deloaded TTG in operational zone 2.

C. MODELLING OF DPP

The power yield from TTG is random in behavior. Thus, for consistent power output to customers, it must be integrated with the diesel power unit. Diesel engine generator comprises a governor, droop controller, and associated controller [4]. The speed governor gives regulated speed by control the feed. On the other hand, primary frequency regulation is provided by droop control, and the PID controller is employed as a secondary controller for enhancing the steady-state response. The DEG in the form of the transfer function is expressed as:

$$G_{DEG}(s) = \frac{1}{(1 + sT_{DG})\,(1 + sT_{DT})} \quad (4)$$

where T_{DG} and T_{DT} are the time constants of the governor and turbine correspondingly.

III. FRACTIONAL CALCULUS-BASED CONTROL STRATEGY

In the present microgrid models, Fractional order (FO) PID controllers are used to control the ΔF. In FO controller, differential equations are solved by fractional calculus (FC). FC is the generalization of the ordinary calculus utilizing the goodness presented by the non-integer order of the Laplace variable s. The fractional integrodifferential operator expresses it, D^i (5) [28].

$$D^i = \begin{cases} \dfrac{d}{dt^i} & i > 0 \\ 1 & i = 0 \\ \int_0^t (d\tau)^{-i} & i < 0 \end{cases} \quad (5)$$

where 'i' is the order of integrator/differentiator. The frequently employed definitions in fractional calculus are Riemann Liouville, Grunwald Letnikov, and Caputo. Caputo's definition is used for control-related problems, written in equation (6) [28].

$$D^i f(t) = \frac{1}{\Gamma(n-i)} \int_0^t \frac{D^n f(\tau)}{(t-\tau)^{i+1-n}} \quad i \in \mathbb{R}^+, \quad n \in \mathbb{Z}^+, \; n-1 \le i < n \tag{6}$$

A. FRACTIONAL-ORDER CONTROLLERS

The fractional calculus uses integration and differentiation with a fractional-order or complex order. The major advantage of a fractional derivative is the ability to inherit the nature of the processes. The FO-PID in the form of the transfer function is written in (7) [28]:

$$\text{Controller response(y)} = D_a \Delta F + K s^{-\lambda} \Delta F + M_a s^{\mu} \Delta F \quad (0 < \lambda \le 1, 0 < \mu \le 0) \tag{7}$$

It has three gain constants; D_a is a proportional part, K is an integral part and M_a is a derivative part with two fractional operators are λ and μ. FOPID controller output "y" is multiplied with (1 + PI) controller to get the final output of the proposed FOPID-(1 + PI) controller, as explained in the given Eq. (8) [11].

$$\Delta u = \left[\left(D_a \Delta f + K s^{-\lambda} \Delta F + M_a s^{\mu} \Delta F\right)\right] \left[\left(1 + K_P + K_i s^{-1}\right)\right] \tag{8}$$

Generally, fractional-order (FO) differentiator and integrator are linear filters of infinite dimensions [28]. Thus, for practical realization, its band-limited implementation is required. One of the perceived approximations is offered by Oustaloup is used in this study. The Oustaloup filter gives an excellent fitting to the fractional-order elements within a chosen frequency range (w_b, w_h) and order N [29].

Further, the sub-optimum H_2 approximation method is exploited to reduce the order of rational transfer function.

The transfer function of the outstaloup filter, zeros, poles, and gain is written in equations (9-12) [29].

$$G_{Outstaloup_{filter}}(s) = K \prod_{l=-n}^{n} \frac{s + w_l'}{s + w_l} \tag{9}$$

$$w_l' = w_b (w_h/w_b)^{\frac{l+N+\frac{1(1-\beta)}{2}}{2N+1}} \tag{10}$$

$$w_l = w_b (w_h/w_b)^{\frac{l+N+\frac{1(1+\beta)}{2}}{2N+1}} \tag{11}$$

$$K = w_h^{\beta} \tag{12}$$

where '2N + 1' is the order of filter and β is the order of integrator/differentiator. In this paper, 5th order Oustaloup's approximation in the frequency range of $\omega\varepsilon\left\{10^{-2}, 10^{2}\right\}$ radian /s for the entire FO elements is used.

IV. DELOADED OPERATION OF TPP

An adequate power reverse margin is needed to offer the essential frequency cooperation from TPPs in transient conditions. Accordingly, TPP might be worked with deloaded from maximum power point operation under different speed conditions [4]. The deloaded TPP operation might be acknowledged either under or over speed. In this research study, deloading activity is done in over speed mode for executing the investigation. There is a specific point in deloaded operation where the turbine's speed escalates over the acceptable limit. It is harmful to the lifecycle of the turbine. The pitch angle control strategy comes into action to resolve this issue, and the pitch controller comes into operation. A detailed description of the pitch angle control strategy is given in [4].

V. INERTIA, DAMPING AND SUPPLEMENTARY CONTROL

In a traditional power generator, the rotor speed is closely related to system frequency. Hence, whenever some disturbance occurs in load and supply, the accumulated kinetic energy presented in DPP emits or stores power speedily to decrease the ΔF through the primary regulation. Thus, the inertia of the DPP constraints the Δf. Due to the random behavior of tidal wave's flow in TPP, permanent magnet synchronous generators/double-fed induction generators (DFIG) are essentially employed by some power electronic interface. Thus, it increases the power reverse margin, but on the other hand, it demotes the overall inertia of the system. The frequency regulation focused on primary controlling strategy (inertial support) in a single and multi-area system, integrated with TPP turns into an imperative assignment. To improve the primary transient response of unpredicted ΔF, the proposed control strategy (i.e., integration of extra inertia, damping, and supplementary control with the deloaded TPP is presented in Figure 6a. Inertia constant might be characterized as the time taken by generator units to deliver power from its accumulated kinetic energy. Whenever there is a large amount of inertia value, the system is more robust to ΔF. The inertia of a specific turbine generator might be communicated by Eq.(13) [30].

$$H = 0.5 J \omega^2 / S \tag{13}$$

where J/ω represents the inertia (kgm^2) / angular speed (rad/s) of the turbine, and S means the rating of the generator system (MW). The estimate of inertia constant for TPP is calculated on its base (1 MW), and it is equal to 0.1939sec. On the other hand, the value of inertia constant of mostly conventional generator units are lie in the limit of 2-9 sec [31] and for wind turbine generator, it is lie in between 2-6 sec [32]. The estimations of parameters of the considered TPP system are given in Appendix [10], [33]. In contrast with the conventional generator unit and wind power turbine, the inertia of TPP is seen as exceptionally low. In this manner, the accessible power reverse limit is more diminutive. The estimation of tidal turbine time constant (T_{TT}) is determined by (14) [34].

$$T_{TT} = J \omega_r / 3 T_r \tag{14}$$

where J, ω_r, and T_r represent the turbine's inertia (kgm^2)/ rated rotor speed (radian/sec)/ rated torque respectively. The value of T_{TT} is equal to 0.08 s by using the above Eq. (14).

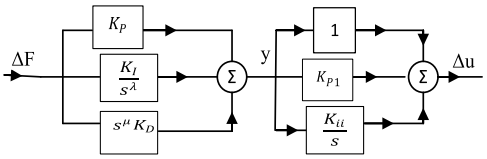

FIGURE 5. Block diagram of FOPID (1 + PI) controller.

The integration of TPP with the DEG system has changed the system's net inertia constant because it is determined by inertia constants of DEG unit/TPP and contribution level of (P_{TPP}) TPPs. The total estimate of inertia constant with the contribution of TPP might be written as Eq. (15) [35].

$$\textit{Total inertia estimate} = \textit{value of inertia constant of DEG}\,(1 - P_{TPP}) \quad (15)$$

In the same context, the damping coefficient (D) value is also an essential factor in characterizing frequency analysis. The impact of additional damping on frequency regulation in wind power plants is discussed in [9] and in the conventional power plant [36]. The combination of additional damping/additional inertia/supplementary control is indicated in Figure 6 (a). The output signal of these combination (ΔP_{di}) is added to the reference power yield to be followed by the non-conventional machine equivalent controller. These control strategies improve the performance analysis of frequency response during the transient period. It is represented by two signals, i.e., Δf and $\partial\Delta$f /∂t in (16) [8].

$$\Delta P_{di} = D_a \Delta F + M_a \frac{\partial \Delta \mathrm{F}}{\partial t} \quad (16)$$

To demote the impact of continuous frequency deviation (Δf), a washout filter is employed on frequency control methodologies. When the transient period is over, the TTG has to recapture the optimized speed again. For attaining the optimal speed, a power reference (ΔP_m, in pu) is used. It is calculated by equation (17) [8], where K_{ps} and K_{is} represent the speed regulator gains.

$$P_m = k_{ps}\left(w^*_{ref} - w_m\right) + k_{is}\int\left(w^*_{ref} - w_m\right)dt \quad (17)$$

Equation (16) reveals that the additional Ma and Da controlling strategy aid in enhancing the transient characteristics, and supplementary control enhances the steady-state response. These control strategies are implemented by employing a fractional PID controller whose parameters are tuned by applying ICA.

VI. DYNAMIC LFC MODEL OF TPP

The Tidal power output variations are written in (18) [37]:

$$\Delta \mathrm{P_{TT}} = \Delta\beta \frac{\mathrm{dp}}{\mathrm{d}\beta} + \Delta\omega \frac{\mathrm{dp}}{\mathrm{d}\omega} + \Delta \mathrm{V}_{TT} \frac{\mathrm{dp}}{\mathrm{dV}_{TT}} \quad (18)$$

where $\frac{\mathrm{dp}}{\mathrm{d}\beta}$, $\frac{\mathrm{dp}}{\mathrm{d}\omega}$, $\frac{\mathrm{dp}}{\mathrm{dV}_{TT}}$ represent the tidal power output perturbation for an inevitable change in pitch angle, change in turbine angular speed, and tidal speed. All these terms are obtained by the following Eq. (19)-(23) [37].

$$\frac{dp}{d\beta} = \frac{1}{2}\rho A_{TT} V_{TT}^{33} \frac{dc_P}{d\beta} \quad (19)$$

$$\frac{dc_p}{d\beta} = 0.167 sin \frac{\pi\,(\lambda_{TT} - 2)}{0.3\beta - 13} - \left[\frac{0.3\pi\,(\lambda_{TT} - 2)}{(0.3\beta - 13))^2} \times cos\left(\frac{\pi\,(\lambda_{TT} - 2)}{(0.3\beta - 13)}\right) \times (0.167\beta - 0.44)\right] - 0.00184\,(\lambda_{TT} - 2) \quad (20)$$

$$\frac{dp}{d\omega} = \frac{1}{2}\rho A V_{TT}^3 \frac{dc_p}{d\lambda_{TT}} \frac{d\lambda_{TT}}{d\omega} \quad (21)$$

$$\frac{dc_p}{d\lambda_{TT}} \frac{d\lambda_{TT}}{d\omega} = \left[\frac{R}{V_{TT}}\right] \frac{\pi}{(0.3\beta - 13)} \times cos \frac{\pi\,(\lambda_{TT} - 2)}{(0.3\beta - 13)} \times (0.167\beta - 0.44) - 0.00184\beta \quad (22)$$

$$\frac{\mathrm{dp}}{\mathrm{dV}_{TT}} = \frac{3}{2}\rho \mathrm{AC_p} V_{TT}^2 \quad (23)$$

The power fluctuations ($\Delta \mathrm{P_{TT}}$) are integrated into the microgrid utilizing additional inertia, damping, and supplementary control signal with the speed controller signal.

The variation in the rotor speed $\Delta\omega_{\mathrm{ref}} - \Delta\omega$ is taken as a signal to the pitch control block for adjusting the estimated angle and rotor speed control block for determining the Pref as shown in Figure 6(a). The load frequency models of the single\two-area microgrid with TPP have appeared in Figures. 6a and b, respectively. The single line graph of two area microgrids appears in Figure 6c.

VII. FITNESS FUNCTION

The initial step for implementing any optimization technique for controller design is to define the fitness function. A literature survey reveals the four performances index in controller design as Integrated Absolute Error (IAE), Integrated Time Absolute Error (ITAE), Integrated Square Error (ISE), and Integrated Time-weighted Square Error (ITSE) [18]. In this study, an integral time absolute error has been taken as a fitness function for finding the controller's optimal parameter. It is written in equation (24) for single area microgrid and two areas interconnected microgrid in equation (25) [38].

$$J_{min} = \int_0^T t.\,(|\Delta F|).dt \quad (24)$$

$$J_{min} = \int_0^T t.\,(|\Delta F_1| + |\Delta F_2| + |\Delta P_{tie}|).dt \quad (25)$$

Minimize J, Subject to a range of adopted controller:

$$K_G^{\min} \le K_G \le K_G^{\max}$$

Here, min and max represent the minimum and maximum values of controllers' parameters, and ΔF_1 / ΔF_2 (in pu) denote the ΔF in area-1/ in area-2, and ΔP_{TIE} (in pu) represent the tie-line power interchanged. IAE, ISE, and ITSE fitness functions are also determined for measuring performance.

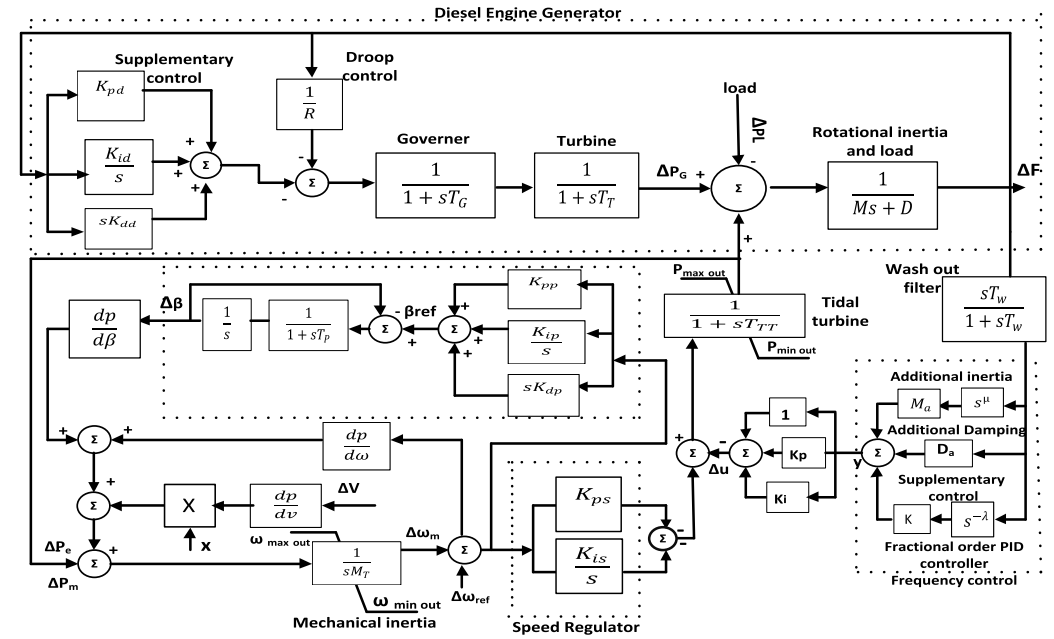

(a)

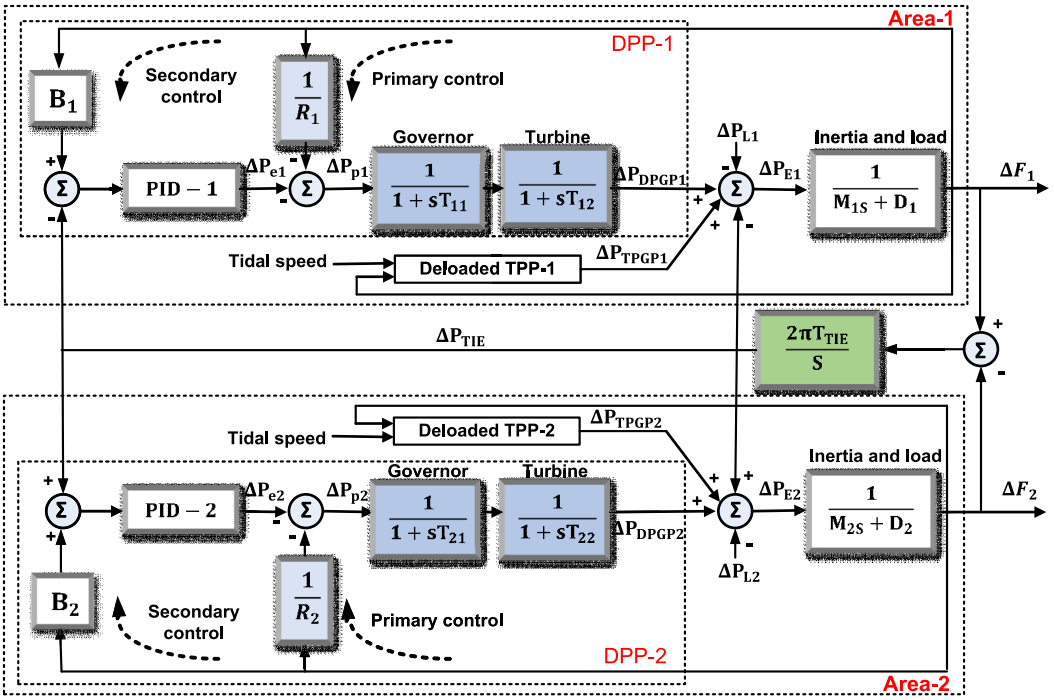

(b)

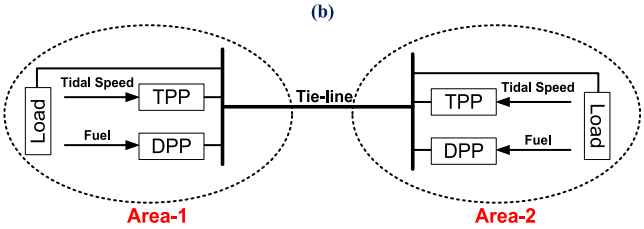

(c)

FIGURE 6. Investigated TPP model: (a) transfer function based single-area Microgrid system, (b) transfer function based two-area Microgrid system, (c) single line diagram of the interconnected proposed model.

VIII. IMPERIALIST COMPETITIVE ALGORITHM

The evolutionary algorithms perceive better result achievements over the standard gradient-based procedures experienced in controller design in the power system. ICA is an advanced metaheuristics optimization technique that speaks to imperialism's social and political advancements and imperialistic competition [24]. It emulates the political/social aura of imperialist countries in an undertaking to oversee the weak countries. ICA begins with an arbitrary populace. Every populace is known as the country. According to their strengths, the countries separate into different imperialists and colonies making a few empires. Each empire involves few colonies and a single colonialist. The imperialistic competition (IC) among colonies builds up the cause of ICA. These empires start to develop simultaneously by pushing all colonies in colonialists' vicinity by an activity named assimilation. In the period of IC, weak colony collapse and compelling ones grab responsibility for provinces.

Finally, IC meets a condition where only one empire exists with their colonies, which has the equal level and cost as the imperialist [24]. Contrasted with different metaheuristics calculations, ICA has various advantages: fast convergence speed, less reliance on an introductory solution, less computational time with little computational expense, strong neighborhood search capacity, minor probabilities of catching into local minima and, many more. Above mentioned advantages motivate to employ ICA in this examination to optimize the gains of the proposed controllers. The initial ICA parameters are given as: countries = 200, iterations = 100, revolution rate (p_r) = 0.3, assimilation coefficient (β) = 1.5, assimilation angle coefficient (ϕ) = 0.5, and coefficient related to average power of emperor's colonies (ξ) = 0.05, the flow chart of ICA have been given in Figure 7.

IX. SIMULATION AND RESULTS

ICA is employed to find a secondary controller's optimal design parameters coupled to DEG and primary frequency regulation control strategy. It is realized by deloaded operation and fractional calculus-based inertia, damping, and supplementary control. To investigate the performance of the studied control strategy for TPP integration, two distinct microgrid models (single-area and two-areas) have been examined. In the presented MG systems, capacities of TPP /DPP are of 1 MW/5 MW taken. With the system base of 5 MW, inertia constants of DPP and TPP are determined as 5 and 0.03878 sec, respectively [4] and employed in the studied Simulink environment. Various parameters related to microgrid models are determined [40] and are given in Table-8 (Appendix). TPP is considered to be working with a 15 percent deloaded limit at a tidal speed of 2.4 meters/sec, with a pitch angle tuned at 3°. The performance of frequency response (alluded as situations) is completed on the proposed microgrid models. The following two case studies of standalone microgrids have been investigated.

Case A: Single-area microgrid.

Case B: Two-area microgrid.

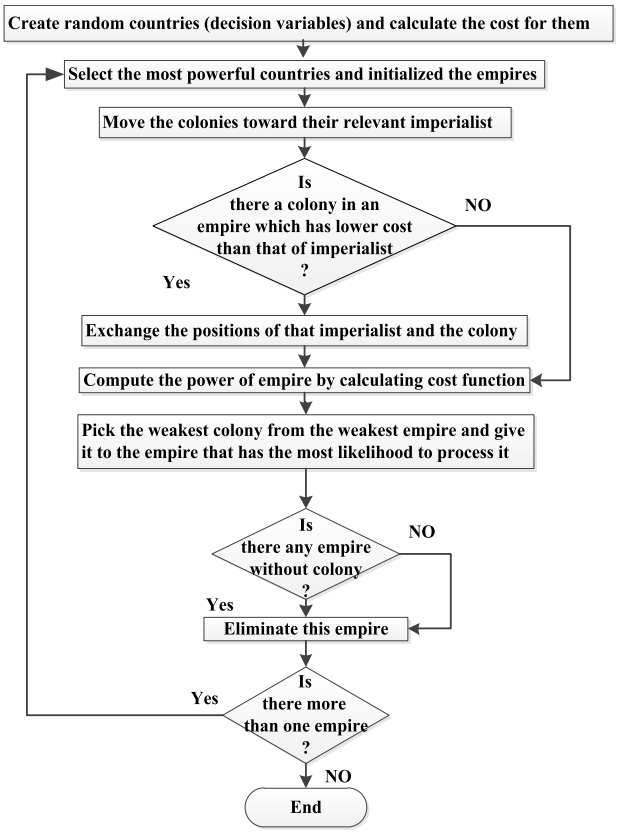

FIGURE 7. ICA Flow chart.

A. DYNAMIC ANALYSIS OF CASE 'A'

In this case, a standalone single-area microgrid is studied for frequency regulation, as shown in Figure 6a. The dynamic analysis of the frequency response for the studied microgrid for this case is investigated under two conditions as given below:

Condition (i): A step load perturbation

Condition (ii): A step perturbation in load and tidal speed.

The value of the studied single-area microgrid parameters is given in Table 8 (Appendix).

1) CASE 'A' (CONDITION (i)): A STEP LOAD PERTURBATION

In this case, only 5% of Step Load Perturbation (SLP) Δ_L) is considered at t = 5 s, and there is no perturbation in tidal speed Δv) is considered. Under this condition, five control schemes have been implemented in MATLAB simulation. The first two schemes are based upon fractional calculus-based (dual stage FOPID (1 + PI) and FOPID) control approaches (alludes to adding inertia, damping, and supplementary control). The third and fourth scheme is conventional PID control and PD employed to adding inertia and damping control. In comparison, the fifth one is without any control approach.

The selection of proper control schemes for efficient system performance depends on the system's complex configuration. Thus, the present system's dynamic performance analysis is done with PID, FOPID, and FOPID (I + PI)

TABLE 1. Tuned design variables of the proposed MG with PID/FOPID/FOPID-(1 + PI) for condition 1 with case A.

Algorithm	Control Structure	Droop Controller's Parameters							pitch controller gain			Speed regulator gain		DPP's controller gain		
		M_a	D_a	K	μ	λ	K_p	K_i	K_{pp}	K_{ip}	K_{dp}	K_{ps}	K_{is}	K_{pd}	K_{id}	K_{dd}
GA	PID	6.89	54.9	40.7	-	-	-	-	1.75	5.42	6.23	4.21	5.42	13.68	6.23	15.08
	FOPID	9.07	48.8	36.9	0.290	0.39	-	-	2.10	5.4	6.13	2.40	7.23	11.6	9.87	12.8
	FOPID(1+PI)	10.56	36.9	31.7	0.30	0.41	24.8	5.9	2.95	6.12	7.05	3.11	6.89	15.79	7.45	14.7
PSO	PID	17.8	83.08	42.09	-	-	-	-	5.32	3.89	6.50	2.94	5.21	14.45	6.96	16.67
	FOPID	19.8	69.03	88.6	0.438	0.52	-	-	7.10	4.89	8.34	3.21	4.85	25.0	6.98	18.4
	FOPID(1+PI)	15.76	75.14	74.8	0.501	0.47	31.4	7.34	6.56	3.63	7.08	2.89	5.08	22.28	5.73	16.8
ICA	PID	78.3	98.6	92.0	-	-	-	-	5.34	4.98	7.32	5.07	4.20	18.09	16.09	15.7
	FOPID	100.3	121.9	96.8	0.642	0.59	-	-	3.9	5.99	6.80	4.09	2.08	19.8	18.9	26.0
	FOPID(1+PI)	93.3	102.7	78.0	0.562	0.48	47.1	5.86	5.02	6.08	8.12	3.88	3.19	20.64	19.45	19.9

TABLE 2. The figure of merit and Transient response parameter of the system with PID/FOPID/FOPID (1 + PI) control under different algorithms.

Studied algorithm		Figure of merit	Transient response of Δf		
	Controller structure	ITAE ($\times 10^{-4}$)	Undershoot ($\times 10^{-4}$pu)	Peak time(sec)	Settling time (sec)
GA	PID	1.72	-4.01	5.59	18.03
	FOPID	1.67	-3.67	5.54	17.22
	FOPID(1+PI)	1.54	-1.71	5.55	12.34
PSO	PID	0.548	-3.70	5.57	17.56
	FOPID	0.2540	-2.14	5.49	17.14
	FOPID(1+PI)	0.221	-0.59	5.49	12.20
ICA	PID	0.249	-1.08	5.57	16.78
	FOPID	0.1094	-0.954	5.39	16.24
	FOPID(1+PI)	0.0956	-0.32	5.36	12.09

TABLE 3. Statistical analysis of different algorithm.

Optimization Technique	Controller Structure	Statistical parameters of J	
		μ	σ
GA	PID	3.1×10^{-6}	5.62×10^{-6}
	FOPID	0.42×10^{-6}	0.58×10^{-6}
	FOPID-(1+PI)	0.1472×10^{-6}	0.031×10^{-6}
PSO	PID	0.956×10^{-6}	0.972×10^{-6}
	FOPID	0.38062×10^{-6}	0.167×10^{-6}
	FOPID-(1+PI)	0.1394×10^{-6}	0.0432×10^{-6}
ICA	PID	0.198×10^{-6}	0.032×10^{-6}
	FOPID	0.0532×10^{-6}	0.0182×10^{-6}
	FOPID-(1+PI)	0.0222×10^{-6}	0.013882×10^{-6}

controllers using GA/PSO/ICA. The optimal design gains (as achieved by using GA/PSO/GOA) of PID, FOPID, and FOPID-(1 + PI) controllers are given in Table 1. The corresponding values of J_{min}, peak overshoot, peak undershoot, and settling time in ΔF, are listed in Table 2. Figures 8 (a)-(c) and Tables 2 report that the exceptional values of J_{min} (ITAE = 0.0956), settling time (12.09 s), peak undershoot (−0.32pu), and peak time (5.36s) is offered by the FOPID-(1 + PI) controller in compared to PID/FOPID controller with considered optimization algorithms. To display the preeminence of ICA with the proposed approach), the outcomes given by it are contrasted with outcomes acquired utilizing another contemplated method, for example, GA and PSO. Their convergence graphs are shown in Figures. 9(a)–(c). Figure 9 reveals that ICA has fast convergence in comparison to PSO and GA. Due to this, online tuning of these controllers is possible in the future. The statistical report of GA, PSO, ICA for PID, FOPID, and FOPID (1 + PI) controllers is specified in Table 3. The ICA algorithm achieves the best value of Jmin for FOPID (1 + PI) compared to PSO and GA, as reported in Table 2. Also, the value of mean (μ) and standard deviation (σ) of the ICA are lowest compared to the GA and PSO as specified in Table 3. It shows reliable and steady outcomes every time. Furthermore, the values of fitness function index and performance indices acquired (for example, ITSE, IAE, and ISE) utilizing various optimizing methods are depicted in Table 4. It again shows the ICA-based FOPID (1 + PI) controller offers the best outcomes evaluated to other studied algorithms/controller. Thus, for further exploration of the MG, just ICA-based FOPID and FOPID (1 + PI) controllers are taken owing to their comparable outcomes.

The characteristics of ΔF and power output variations noticed in TTG and DEG employing different controlling schemes are shown in Figures 10(a) –(c). Fig. 10 (a) shows that the maximum ΔF has come to −0.000515 p.u. along with considerable settling time, and in the same line, Figure 10 (c) reveals that TTG offers no participation with no control scheme. With the PD control scheme, the TTG integrated additional inertia and damping. It improves the outcomes, the maximum ΔF lessens to −0.00035 pu, and with

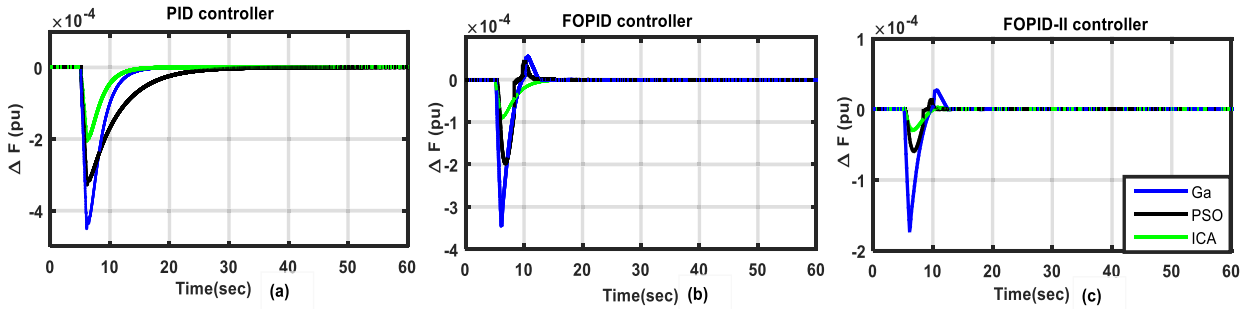

FIGURE 8. Frequency deviation curve considering different algorithms under (a) PID (b) FOPID (c) FOPID(1 + PI) under Case 'A' (condition-i (step load perturbation)).

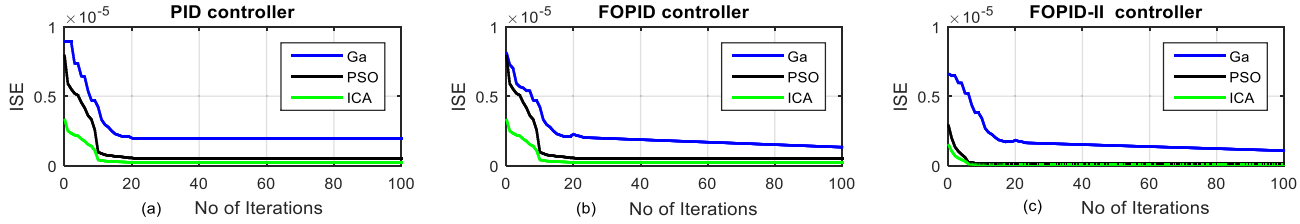

FIGURE 9. Convergence characteristics profiles with different algorithms under (a) PID (b) FOPID (c) FOPID(1 + PI) under Case 'A' (condition-i (step load perturbation)).

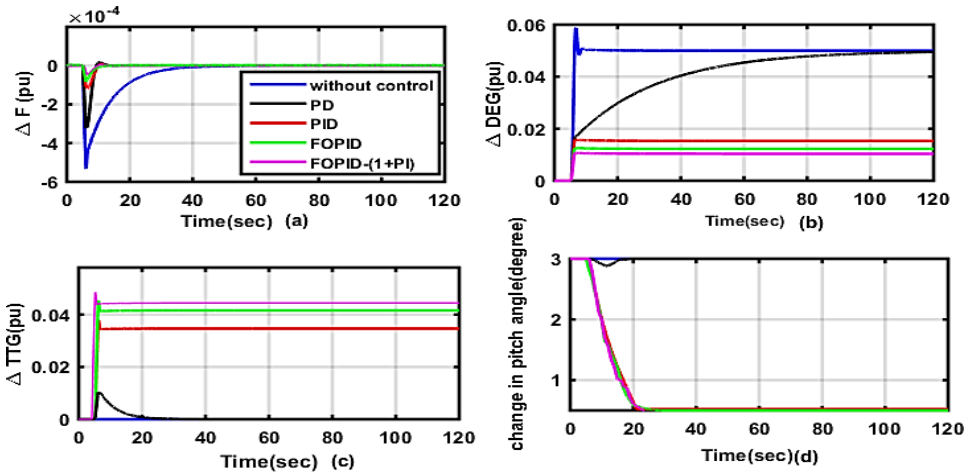

FIGURE 10. Output profiles signal acquired with different control scheme referring to Case 'A' (Condition-i (step load perturbation)).

PID/FOPID control scheme, maximum frequency deviation comes to 0.000167pu/-0.00005pu. The dual-stage FOPID (1 + PI) control scheme is executed to facilitate the frequency regulation. Figure 10 (a) reveals that the FOPID (1 + PI) control scheme imparts enough power to the MG to improve the transient and steady-state characteristics.

The maximum value of ΔF is -0.000042 pu obtained, which is the lowest compared to other studied schemes. Moreover, it takes less settling time, thus enhances the power quality. The output power plots (TTG and DEG) align with the results displayed in Figures 10 (b) and (c). It may be observed from these plots that in the absence of control schemes, support from the TTG is zero, and DEG proceeds the entire burden. In the case of inertial and damping control (PD control), the TTG injects inertia in the beginning to provide frequency support. The TTG does not change the output power in a steady-state condition. However, it improves the transient characteristics as overshoot, undershoot, and settling time, as displayed in Figure 10 (a). Figure10 (b) shows that TTG transiently gives the maximum power injection of 0.012pu for a few seconds and supports zero after 25s. In control scheme (iii), i.e., PID control, the output power via TTG changes smoothly and rises continuously to a fixed value of 0.038pu. The flat slope of the power yield plot in TTG is noticed owing to the reserved power margin present inside it. While in the beginning, DEG offers power to support the load immediately and obtain the peak power deviation of 0.045pu. After the transient period is completed, its steady-state values come down to 0.014pu, as observed in Figure 10 (b). Owing to the inclusion of the

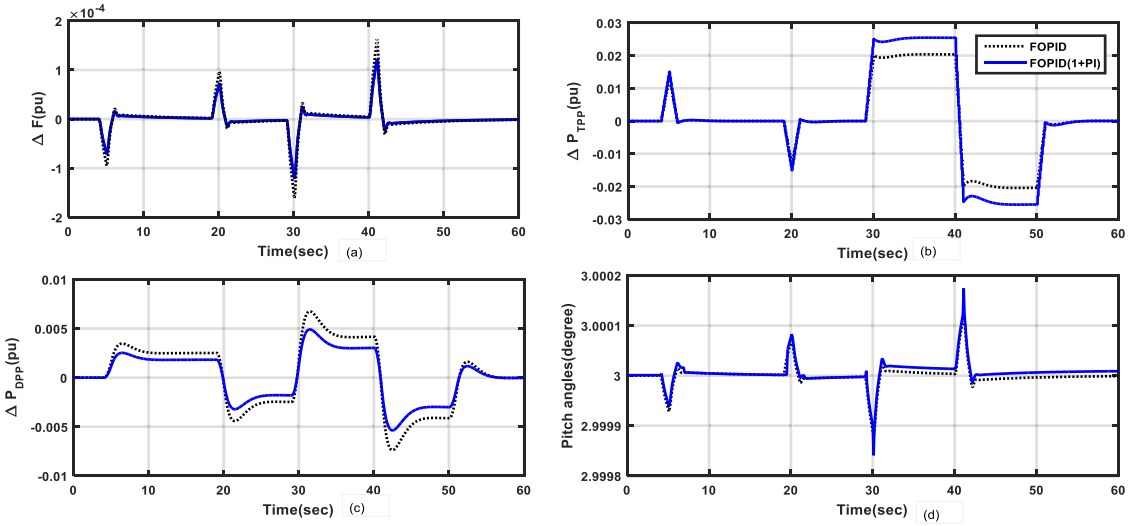

FIGURE 11. Output profile signals under Case 'A' (Condition -ii (step perturbation in both load demand and tidal speed.

TABLE 4. Fitness function estimate & performance indices acquired with PID/FOPID/FOPID (1 + PI) control under different algorithms (Case 'A'-condition i).

Studied algorithm	Controller structure	ITAE ($\times 10^{-4}$)	ITSE ($\times 10^{-8}$)	IAE ($\times 10^{-4}$)	ISE ($\times 10^{-8}$)
GA	PID	1.72	6.01	1.37	2.07
	FOPID	1.67	5.56	1.02	1.98
	FOPID(1+PI)	1.54	5.21	0.914	1.65
PSO	PID	0.548	4.72	1.087	1.64
	FOPID	0.2540	4.29	0.945	1.090
	FOPID(1+PI)	0.221	4.02	0.9109	1.005
ICA	PID	0.249	1.98	0.521	1.098
	FOPID	0.1094	1.69	0.495	0.908
	FOPID(1+PI)	0.0956	1.24	0.412	0.674

fractional calculus-based control strategy, the support of the TTG lessens the burden on the DEG and improves the frequency plot, as revealed from Figure 10 (a). As seen from Figure 10(d), no variation in β is observed without control. With inertia and damping control, a transient variation is noticed in the plot of β followed by a load variation in the beginning which achieves the stable condition (initial value) soon after, as seen in Figure.10 (d). In PID, FOPID, and FOPID (1 + PI) based control schemes. It is noticed that the permanent support of power from TTG in frequency control varies the value of β from 3^0 to 0.50^0.

2) CASE A (CONDITION (ii)): A STEP PERTURBATION IN BOTH LOAD DEMAND AND TIDAL SPEED

In this case study, the increment and afterward abatement of 1.5% SLP is given at t = 5 sec, and t = 20 sec individually. Additionally, the single-area microgrid is exposed to initially diminish and afterward increment of 0.05 meter/sec in tidal speed at t = 30 sec and t = 40 sec, individually. Since it has been seen in the condition (i) of Case 'A,' the response of frequency regulation for the fractional calculus-based control scheme is superior compared to without it. Henceforth, both fractional calculus-based control schemes are used for getting the simulation results for this situation. In this condition, the gains of previously tuned controllers are employed, and no further tuning of the controller is conducted.

The comparable response signals of frequency deviation, power output from TPP and DPP, and pitch angle acquired after applying the perturbations mentioned above have appeared in Figure 11. Figure 11(a) reveals that after subsequent increment and decrement in SLP, system frequency drops and recovers its base value with the proposed scheme. An instant change appears in the profile of ΔP_{TPP} as shown in Figure 11(b), which indicates the temporary support of TPP in frequency control via additional inertia. Thus, an increase or decrease in demand will only affect the DPP yield, as reveals in Figure 11(c). At t = 30 sec, tidal speed reduces (either 0.05 m/sec), P_{TPP} diminishes, and at the same time, an increment in power yield from DPP is observed. Similarly, observations are noticed at t = 40 sec when the following rise in tidal speed occurs. It is seen from Figure 11(d) that the deloaded TPP reacts (as variation in pitch angle) according to changes in load and tidal speed.

B. DYNAMICS ANALYSIS UNDER CASE 'B'

In this case, the frequency response investigation of a two-area microgrid system (appeared in Figure 6(b) has been examined, with both the areas are supposed the same. The proposed frequency response analysis is carried out with both FOPID/FOPID-II control schemes. The system is tested by four conditions of implementing different perturbations in area-1. The proposed conditions are given below.

TABLE 5. FOPID Controller's parameters of two areas microgrid model with 5%SLP in area -1(Case 'B'-condition (i)).

Studied Algorithm	Control Area	Proposed Controller gain					Pitch controller gain			Speed regulator gain		DPP's controller gain		
		M_a	D_a	K	μ	λ	K_{pp}	K_{ip}	K_{dp}	K_{ps}	K_{is}	K_{pd}	K_{id}	K_{dd}
GA	1	10.56	72.5	65.01	0.82	0.61	0.004	8.76	22.02	13.45	11.08	18.08	54.2	7.34
	2	7.81	67.2	52.8	0.67	0.54	0.003	5.34	21.9	8.79	5.23	23.09	56.4	5.31
PSO	1	92.06	66.3	96.08	0.678	0.72	0.002	9.72	25.89	7.67	9.14	17.59	45.62	2.6
	2	87.09	98.2	34.89	0.78	0.32	0.002	15.98	26.12	9.51	8.67	18.05	20.09	16.89
ICA	1	79.3	88.9	53.2	0.68	0.57	0.008	7.09	9.29	5.61	10.01	47.07	56.9	14.9
	2	43.89	45.2	46.3	0.29	0.79	0.006	16.09	8.48	3.09	9.07	20.78	8.67	5.90

TABLE 6. FOPID-II Controller's parameters of two areas microgrid model with 5%SLP in area -1(Case 'B'-condition (i)).

Algorithm	Control Area	proposed Controller gain					Pitch controller gain			Speed regulator gain		DPP's controller gain		
		M_a	D_a	K	μ	λ	K_p	K_i	K_{pp}	K_{ip}	K_{dp}	K_{ps}	K_{is}	K_{pd}
GA	1	18.09	88.2	73.42	0.65	0.45	44.89	2.09	0.0039	9.04	19.56	12.12	10.34	19.16
	2	9.64	59.9	72.6	0.59	0.85	32.6	5.9	0.0032	8.09	24.2	7.69	8.89	40.11
PSO	1	88.97	48.4	87.96	0.75	0.86	32.04	4.98	0.00178	8.53	24.06	6.21	7.48	13.25
	2	90.32	91.1	51.67	0.54	0.512	38.5	6.89	0.0015	6.87	29.08	8.74	9.07	20.56
ICA	1	67.9	56.7	55.3	0.73	0.49	53.90	9.89	0.010	9.21	8.56	4.84	11.78	56.89
	2	52.55	80.2	65.21	0.87	0.57	34.21	2.09	0.0065	12.21	9.082	6.32	8.94	21.64

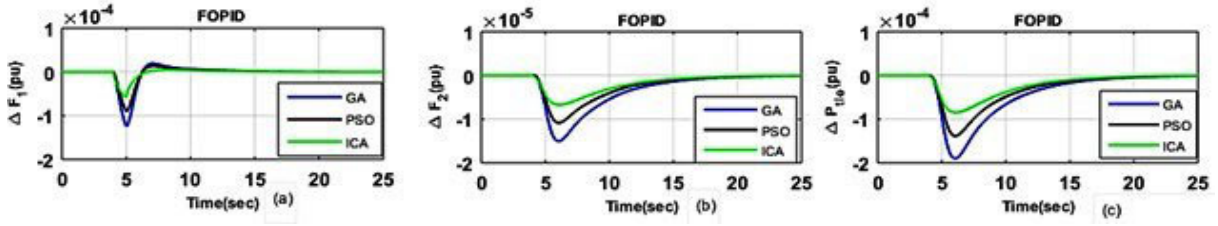

FIGURE 12. Comparative dynamic response of two area microgrid model under condition-(i) for Case 'B' obtained for GA, PSO and ICA optimized FOPID control system.

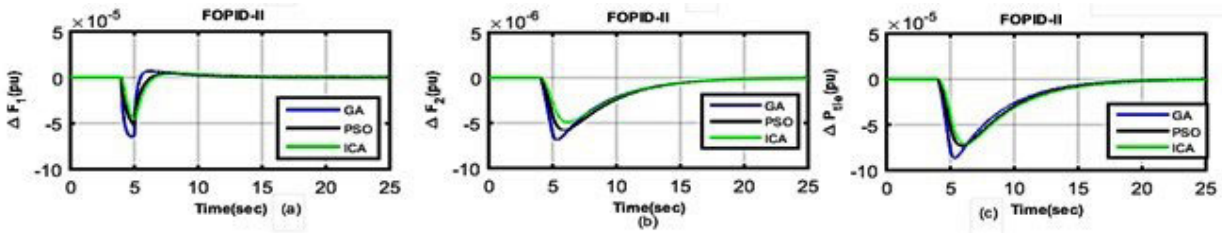

FIGURE 13. Comparative dynamic response of two area microgrid model under condition-(i) for Case 'B' obtained for GA, PSO and ICA optimized FOPID(1 + PI) system.

Condition (i): A step load perturbation.
Condition (ii): Stochastic load perturbation.
Condition (iii): Stochastic tidal speed perturbation.
Condition (iv): Sinusoidal load perturbation.

1) CASE B (CONDITION (i)): A STEP LOAD PERTURBATION

For dynamic analysis of the system, by considering $\Delta v = 0$ and 5% of SLP in area 1 at t = 5sec. The simulation for performance analysis of two area microgrids is conducted under each of GA, PSO, and ICA optimized controllers (related with TPP and DPP of the system). The optimized parameters of FOPID and FOPID(1 + PI) with 5% SLP in area -1 utilizing all considered algorithms are reported in Tables 5 and 6. Their dynamic responses are shown in Figures 12(a)–(c) and Figures 13(a)-(c), respectively. The fitness function estimations and other performance criteria (for example, ITSE, IAE, and ISE) acquired with various calculations are recorded in Table 7. Table 5 indicates that ICA performs best in contrast with different algorithms and gives the best transient response of frequency and tie-line power deviations. Likewise, it offers the best estimation of the fitness function and the other performance criteria records.

2) CASE B (CONDITION (ii)): STOCHASTIC LOAD PERTURBATION

In the above condition, investigation analysis reveals the outperformance of ICA based FOPID (1 + PI) controller. To prove the sturdiness of the ICA optimized FOPID(1 + PI) controller, the controllers with the same values of parameters, as obtained in condition (i) of Case 'B', are utilized for the frequency response analysis of the considered

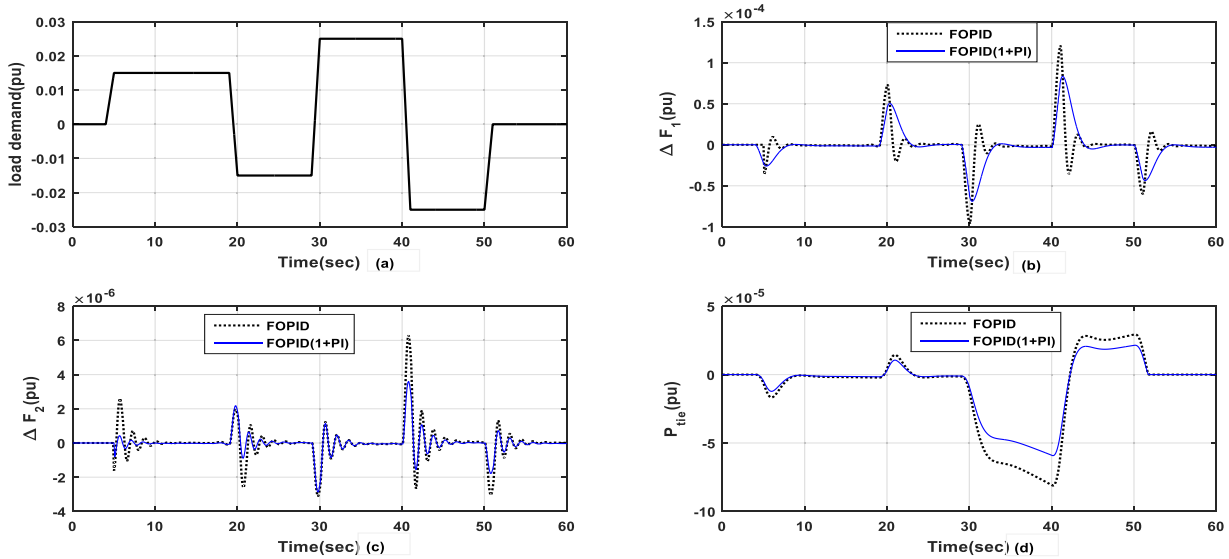

FIGURE 14. Performance analysis of the proposed system with perturbation in load demand (a) load perturbation (b) ΔF_1 (c) ΔF_2 (d) ΔPtie.

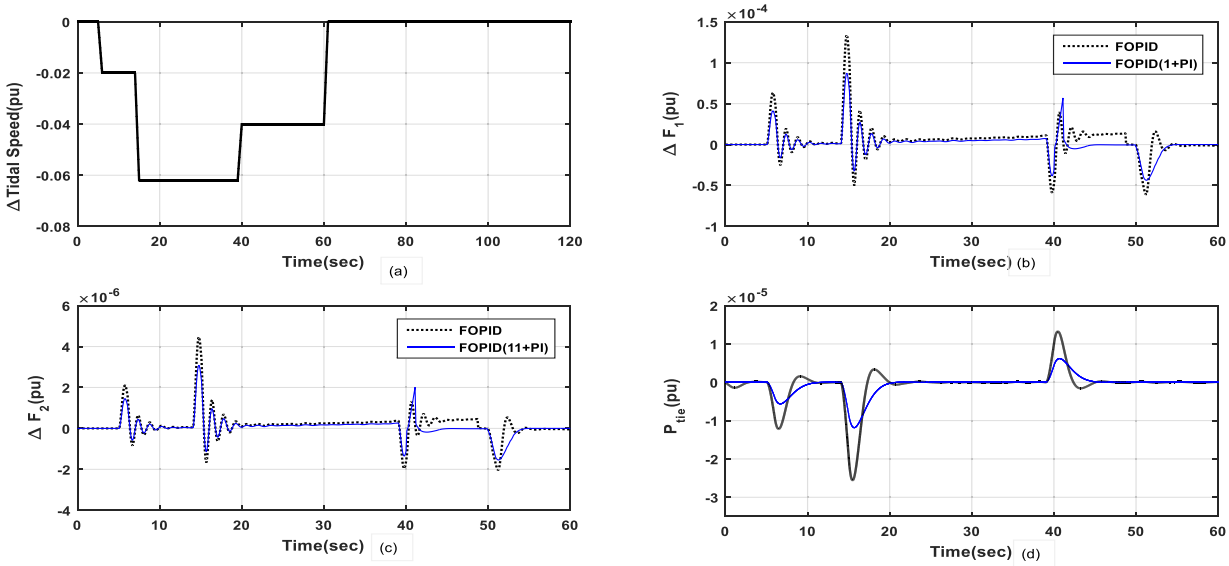

FIGURE 15. performance analysis of the proposed system with perturbation in tidal speed (a) tidal speed perturbation (b) ΔF_1 (c) ΔF_2 (d) ΔPtie.

microgrid model. Figure 14(a) shows the stochastic change in applied load at area 1 of the proposed system and corresponding changes in profiles of ΔF_1, ΔF_2, and ΔP_{tie} with FOPID/FOPID(1 + PI) control schemes are shown in Figures 14b and 14c. The predominance of ICA in damping the system oscillations is visible in outcomes that appeared in Figures 14b, 14c, and 14d. Thus, the results mentioned above again confirm that the optimized estimation of the controllers acquired in condition (i), not required to tune again for significant changes in load.

3) CASE 'B' (CONDITION (iii))

Stochastic tidal speed perturbation: The load change is zero ($\Delta P_L = 0$), and the frequency response analysis is examined by considering solely stochastic variation in tidal speed as appeared in Figure 15a. The corresponding outcome signals of ΔF_1, ΔF_2, and ΔP_{TIE} are depicted in Figures. 15(b) –(d) with FOPID/FOPID(1 + PI) control schemes. The output response reveals that the FOPID(1 + PI) controller has given a stable yield even in the presence of wide stochastic variation in the tidal speed. Thus, it is not required to upgrade the controller as obtained in the previous condition.

4) CASE 'B' (CONDITION (iv))

Sinusoidal perturbation in load demand: In this condition, sinusoidal load employing proposed control methodology is implemented. The sinusoidal load is shown in Fig 16(a).and written in equation (24) [18]:

$$\Delta P_L = 0.002 \sin(4.36t) + 0.005 \sin(5.3t) - 0.01 \sin(6t) \quad (26)$$

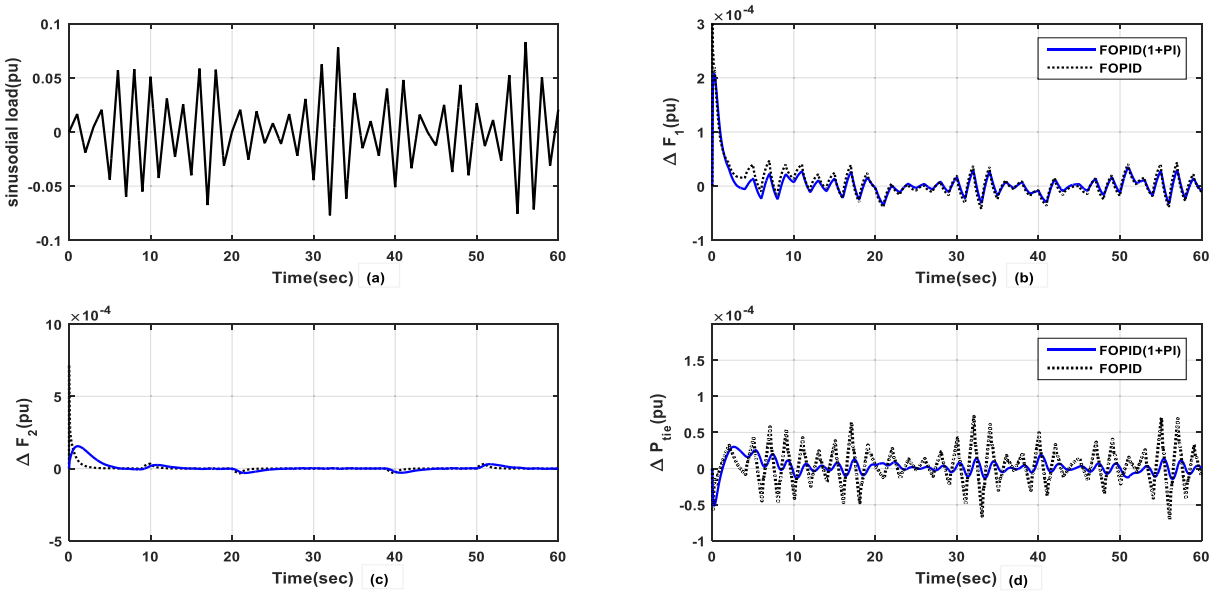

FIGURE 16. Performance analysis with sinusoidal load perturbation. (a)Sinusoidal load perturbation. (b) ΔF_1 (c) ΔF_2 (d) ΔPtie.

TABLE 7. Fitness function estimate performance indices acquired for the proposed model with 5% SLP in area-1under case 'b'-condition (i).

Studied algorithm	Control scheme	ITAE ($\times 10^{-6}$)	ITSE ($\times 10^{-9}$)	IAE ($\times 10^{-4}$)	ISE ($\times 10^{-9}$)
GA	FOPID	4.33	7.963	1.276	2.07
	FOPID(1+PI)	3.79	6.805	1.09	1.69
PSO	FOPID	4.102	7.006	1.105	1.93
	FOPID(1+PI)	3.02	6.765	0.975	1.21
ICA	FOPID	**1.982**	**3.28**	**0.642**	**1.08**
	FOPID(1+PI)	**1.076**	**2.93**	**0.508**	**0.879**

The profiles of ΔF_1, ΔF_2, and ΔP_{tie} are presented in Figures 16(b)-(d), and the same previously mentioned controller's parameters are adopted here again for the analysis. It is observed in Figure.16 that FOPID (1 + PI) control scheme gives superior results in the case of fast load dynamics in terms of frequency regulation.

X. CONCLUSION

In this paper, an exhaustive proposed study of load frequency control with single-area / two-area microgrid models for integrating DPP and deloaded TPP. The inclusion of renewable sources such as TPP (with power electronics interaction to provide stable yield) increases the power capacity. Generally, it reduces the total inertia of the system. Thus, the presented study intends to investigate the frequency regulation through deloaded TPP support. FOPID(1 + PI) control methodology is presented by which additional inertia\damping from deloaded TPP is included in the microgrid model. An exhaustive dynamic performance analysis is done using a considered control methodology for a single/multi-isolated MG system. The effectiveness of the FOPID (1 + PI) control scheme is demonstrated. Also, it compared with other control schemes and obtained $0.2016*10^{-4}$ pu frequency deviation (with proposed scheme) in contrast to $0.245*10^{-4}$/$1.05*10^{-4}$/$3.2*10^{-4}$/$5.89*10^{4}$pu

TABLE 8. Parameters of proposed 2 area microgrid model.

Rated rotor speed (w_r)	13 rpm	Governor time constant (T_G) =T_{G1}=T_{G2}	0.1 s
Tidal speed (V_{TT})	2.4 m/s	Diesel engine turbine (T_T) T_{T1}=T_{T2}	0.25 s
Water density(ρ_{TT})	1027kgm^2	Swept area of rotor (A_{TT})	415m^2
Tip speed ratio (λ_{TT})	6.1	R (droop coefficient) = R1=R2	0.06 pu Hz/MW
Rotor radius (r)	11.5m	Inertia constant M=M1=M2	10
No of blades	3	Damping constant D=D1=D2	0.5 pu MW/pu
Length of blade	10.6 m	F (system frequency)	50 Hz
M_T(=2H_{TPP})	0.0775 s (on 5MW base)	DEG capacity	5 MVA
T_P	0.01s	T_w (wash out filter)	6s
T_r (rated turbine torque)	734753Nm	B1=B2	17.16 pu MW/pu
P_{TIEMAX}	0.4 MW	T_{TIE}	0.07
Tidal Turbine time constant (T_{TT})	0.08 s	TTG capacity	1 MW
Rotor inertia (Jr)	110,688 kgm^2	Rotor blade inertia (J_g)	11986 kgm^2
Generator rotor inertia	86700 kgm^2	Rotor position	upstream

(with FOPID/ PID/ PD/ no control scheme). The parameters of the controllers associated with DPP/TPP are tuned with GA/PSO/ICA. The performances of the optimized controllers are evaluated, the response of ICA optimized controllers is shown notable performance compared to other contemplated techniques. Further, the ICA optimized controllers' effectiveness in reducing ΔF by inertial addition from TPP is similarly checked concerning an extensive change in loads and tidal speeds. Future work will concentrate on the collective contribution of TPP, energy storage units, and DPP in frequency control, and tested new control strategies like cascade control,

tilt integral derivative control, etc., and new algorithms for tuning the parameters of the system.

APPENDIX

See Table 8.

REFERENCES

[1] Y. Tang, Y. Bai, C. Huang, and B. Du, "Linear active disturbance rejection-based load frequency control concerning high penetration of wind energy," *Energy Convers. Manage.*, vol. 95, pp. 259–271, May 2015.
[2] G. Lalor, A. Mullane, and M. O'Malley, "Frequency control and wind turbine technologies," *IEEE Trans. Power Syst.*, vol. 20, no. 4, pp. 1905–1913, Oct. 2005.
[3] Y. Wang, G. Delille, H. Bayem, X. Guillaud, and B. Francois, "High wind power penetration in isolated power systems—Assessment of wind inertial and primary frequency responses," *IEEE Trans. Power Syst.*, vol. 28, no. 3, pp. 2412–2420, Aug. 2013.
[4] K. V. Vidyanandan and N. Senroy, "Primary frequency regulation by deloaded wind turbines using variable droop," *IEEE Trans. Power Syst.*, vol. 28, no. 2, pp. 837–846, May 2013.
[5] N. R. Ullah, T. Thiringer, and D. Karlsson, "Temporary primary frequency control support by variable speed wind turbines—Potential and applications," *IEEE Trans. Power Syst.*, vol. 23, no. 2, pp. 601–612, May 2008.
[6] J. Morren, S. W. H. de Haan, W. L. Kling, and J. A. Ferreira, "Wind turbines emulating inertia and supporting primary frequency control," *IEEE Trans. Power Syst.*, vol. 21, no. 1, pp. 433–434, Feb. 2006.
[7] D. Gautam, L. Goel, R. Ayyanar, V. Vittal, and T. Harbour, "Control strategy to mitigate the impact of reduced inertia due to doubly fed induction generators on large power systems," *IEEE Trans. Power Syst.*, vol. 26, no. 1, pp. 214–224, Feb. 2011.
[8] J. M. Mauricio, A. Marano, A. Gomez-Exposito, and J. L. Martinez Ramos, "Frequency regulation contribution through variable-speed wind energy conversion systems," *IEEE Trans. Power Syst.*, vol. 24, no. 1, pp. 173–180, Feb. 2009.
[9] H. Li, S. Liu, H. Ji, D. Yang, C. Yang, H. Chen, B. Zhao, Y. Hu, and Z. Chen, "Damping control strategies of inter-area low-frequency oscillation for DFIG-based wind farms integrated into a power system," *Int. J. Electr. Power Energy Syst.*, vol. 61, pp. 279–287, Oct. 2014.
[10] B. Whitby and C. E. Ugalde-Loo, "Performance of pitch and stall regulated tidal stream turbines," *IEEE Trans. Sustain. Energy*, vol. 5, no. 1, pp. 64–72, Jan. 2014.
[11] Zaheeruddin and K. Singh, "Intelligent fractional-order-based centralized frequency controller for microgrid," *IETE J. Res.*, early access, pp. 1–15, Mar. 2020, doi: 10.1080/03772063.2020.1730249.
[12] H. Bevrani, G. Ledwich, Z. Y. Dong, and J. J. Ford, "Regional frequency response analysis under normal and emergency conditions," *Electr. Power Syst. Res.*, vol. 79, no. 5, pp. 837–845, May 2009.
[13] C. Pradhan and C. N. Bhende, "Frequency sensitivity analysis of load damping coefficient in wind farm-integrated power system," *IEEE Trans. Power Syst.*, vol. 32, no. 2, pp. 1016–1029, Mar. 2017.
[14] G. Shankar and V. Mukherjee, "Quasi oppositional harmony search algorithm based controller tuning for load frequency control of multi-source multi-area power system," *Int. J. Electr. Power Energy Syst.*, vol. 75, pp. 289–302, Feb. 2016.
[15] I. Nasiruddin, T. S. Bhatti, and N. Hakimuddin, "Automatic generation control in an interconnected power system incorporating diverse source power plants using bacteria foraging optimization technique," *Electr. Power Compon. Syst.*, vol. 43, no. 2, pp. 189–199, Jan. 2015.
[16] K. S. S. Ramakrishna, P. Sharma, and T. Bhatti, "Automatic generation control of interconnected power system with diverse sources of power generation," *Int. J. Eng., Sci. Technol.*, vol. 2, no. 5, pp. 51–65, Sep. 2010.
[17] S. K. Pandey, S. R. Mohanty, N. Kishor, and J. P. S. Catalão, "Frequency regulation in hybrid power systems using particle swarm optimization and linear matrix inequalities based robust controller design," *Int. J. Electr. Power Energy Syst.*, vol. 63, pp. 887–900, Dec. 2014.
[18] A. Kumar and G. Shankar, "Quasi-oppositional harmony search algorithm based optimal dynamic load frequency control of a hybrid tidal–diesel power generation system," *IET Gener., Transmiss. Distrib.*, vol. 12, no. 5, pp. 1099–1108, Mar. 2018.
[19] A. Latif, D. C. Das, A. K. Barik, and S. Ranjan, "Illustration of demand response supported co-ordinated system performance evaluation of YSGA optimized dual stage PIFOD-(1 + PI) controller employed with wind-tidal-biodiesel based independent two-area interconnected microgrid system," *IET Renew. Power Gener.*, vol. 14, no. 6, pp. 1074–1086, Apr. 2020, doi: 10.1049/iet-rpg.2019.0940.
[20] A. Askarzadeh, "Electrical power generation by an optimised autonomous PV/wind/tidal/battery system," *IET Renew. Power Gener.*, vol. 11, no. 1, pp. 152–164, Jan. 2017, doi: 10.1049/iet-rpg.2016.0194.
[21] S. P. Ghoshal, "Optimizations of PID gains by particle swarm optimizations in fuzzy based automatic generation control," *Electr. Power Syst. Res.*, vol. 72, no. 3, pp. 203–212, Dec. 2004.
[22] D. C. Das, A. K. Roy, and N. Sinha, "GA based frequency controller for solarthermal-diesel-wind hybrid energy generation/energy storage system," *Int. J. Electr. Power Energy Syst.*, vol. 43, no. 1, pp. 262–279, 2012.
[23] G. Shankar and V. Mukherjee, "Load frequency control of an autonomous hybrid power system by quasi-oppositional harmony search algorithm," *Int. J. Electr. Power Energy Syst.*, vol. 78, pp. 715–734, Jun. 2016.
[24] G. E. Atashpaz and C. Lucas, "Imperialist competitive algorithm: An algorithm for optimization inspired by imperialistic competition," in *Proc. IEEE Congr. Evol. Comput.*, Singapore, Sep. 2007, pp. 4661–4667.
[25] Y. Arya, "AGC of PV-thermal and hydro-thermal power systems using CES and a new multi-stage FPIDF-(1+PI) controller," *Renew. Energy*, vol. 134, pp. 796–806, Apr. 2019.
[26] Y. Arya, "Effect of energy storage systems on automatic generation control of interconnected traditional and restructured energy systems," *Int. J. Energy Res.*, vol. 43, no. 12, pp. 6475–6493, Oct. 2019.
[27] J. Pahasa and I. Ngamroo, "Coordinated control of wind turbine blade pitch angle and PHEVs using MPCs for load frequency control of microgrid," *IEEE Syst. J.*, vol. 10, no. 1, pp. 97–105, Mar. 2016.
[28] I. Podlubny, "Fractional order systems and PIλDμ controller," *IEEE Trans. Autom. Control*, vol. 44, no. 1, pp. 208–214, Jan. 1999.
[29] A. Oustaloup, F. Levron, B. Mathieu, and F. M. Nanot, "Frequency-band complex noninteger differentiator: Characterization and synthesis," *IEEE Trans. Circuits Syst. I, Fundam. Theory Appl.*, vol. 47, no. 1, pp. 25–39, Jan. 2000.
[30] P. Kundur, *Power System Stability and Control*. New York, NY, USA: McGraw-Hill, 1994.
[31] J. J. Grainger and W. D. Stevenson, *Power System Analysis*. New York, NY, USA: McGraw-Hill, 1994.
[32] K. Hans and J. N. Nielsen, "Introduction to the modelling of wind turbines," in *Wind Power in Power Systems*, T. Ackermann, Ed. Chichester, U.K.: Wiley, 2005, pp. 525–585.
[33] B. Whitby, "Control of an axial flow tidal stream turbine," Ph.D. dissertation, Cardiff Univ., Cardiff, U.K., Aug. 2013.
[34] C. Tang, M. Pathmanathan, and W. L. Soong, "Effect of inertia on dynamic performance of wind turbines," in *Proc. AUPEC*, Sydney, NSW, Australia, Dec. 2016, pp. 1–6.
[35] P. Bhatt, R. Roy, and S. P. Ghoshal, "Dynamic participation of doubly fed induction generator in automatic generation control," *Renew. Energy*, vol. 36, no. 4, pp. 1203–1213, Apr. 2011.
[36] H. Huang and F. Li, "Sensitivity analysis of load-damping characteristic in power system frequency regulation," *IEEE Trans. Power Syst.*, vol. 28, no. 2, pp. 1324–1335, May 2013, doi: 10.1109/TPWRS.2012.2209901.
[37] V. Gholamrezaie, M. G. Dozein, H. Monsef, and B. Wu, "An optimal frequency control method through a dynamic load frequency control (LFC) model incorporating wind farm," *IEEE Syst. J.*, vol. 12, no. 1, pp. 392–401, Mar. 2018, doi: 10.1109/JSYST.2016.2563979.
[38] B. Mohanty, S. Panda, and P. K. Hota, "Controller parameters tuning of differential evolution algorithm and its application to load frequency control of multi-source power system," *Int. J. Electr. Power Energy Syst.*, vol. 54, pp. 77–85, Jan. 2014, doi: 10.1016/j.ijepes.2013.06.029.
[39] Y. Arya, "Effect of electric vehicles on load frequency control in interconnected thermal and hydrothermal power systems utilising CF-FOIDF controller," *IET Gener., Transmiss. Distrib.*, vol. 14, no. 14, pp. 2666–2675, Jul. 2020, doi: 10.1049/iet-gtd.2019.1217.
[40] K. S. S. Ramakrishna and T. S. Bhatti, "Sampled-data automatic load frequency control of a single area power system with multi-source power generation," *Electr. Power Compon. Syst.*, vol. 35, no. 8, pp. 955–980, Aug. 2007, doi: 10.1080/15325000701199479.